# Peripheral Functionalization of Dendrimers Regulates Internalization and Intracellular Trafficking in Living Cells

*Lorenzo Albertazzi,*[a,b]**#* *Marcos Fernandez-Villamarin,*[c#] *Ricardo Riguera,*[c] *and Eduardo Fernandez-Megia*[c]***

[a] NEST, Scuola Normale Superiore and Istituto Nanoscienze-CNR, I-56127 Pisa, Italy; [b] IIT@NEST, Center for Nanotechnology Innovation, Pisa, Italy; [c] Department of Organic Chemistry and Center for Research in Biological Chemistry and Molecular Materials (CIQUS), University of Santiago de Compostela, Jenaro de la Fuente s/n, 15782 Santiago de Compostela, Spain.

L.Albertazzi@tue.nl ; ef.megia@usc.es

**RECEIVED DATE**

TITLE RUNNING HEAD: Periphery of Dendrimers Regulates Cell Internalization

CORRESPONDING AUTHOR FOOTNOTE: Current Address: Lorenzo Albertazzi, TU/e, Den Dolech 2, 5612 AZ Eindhoven, The Netherlands.

# These authors equally contribute to the work.

**ABSTRACT:** GATG (gallic acid-triethylene glycol) dendrimers represent appealing nanostructures for biomedical applications. The incorporation of specific ligands, targeting, and imaging agents on their surface has resulted in promising tools in diagnosis and drug delivery. With the aim of further exploring the versatility of GATG dendrimers in the biomedical field, in this work we study the effect of the peripheral substitution on their uptake and intracellular trafficking in living cells. To this end, peripheral groups with different physicochemical properties and biological relevance have been installed on the surface of GATG dendrimers, and their interactions, uptake efficacy, and specificity for certain cell populations studied by confocal microscopy. Finally, this information was used to design a pH-sensitive drug delivery system for the selective release of cargo molecules inside cells after lysosomal localization. These results along with the easy functionalization and modular architecture of GATG dendrimers reveal these systems as promising nanotools in biomedicine.

**KEYWORDS:** dendrimer, cell internalization, intracellular trafficking, CuAAC, click chemistry

## Introduction

Dendrimers are promising nanostructures for biomedical applications such as drug and gene delivery, diagnosis, and biosensing (*1-4*). Their characteristic monodispersity and tree-like structure endows dendrimers with unique properties such as controlled physicochemical properties and globular morphology. In addition, their inherent multivalency allows for the display of specific ligands, drugs, targeting, and imaging agents (*5-9*). The Vögtle "cascade synthesis" constituted the first strategy towards dendritic structures (*10*). This was followed by reports on polyamidoamine (PAMAM) dendrimers by Tomalia (*11*) and arborols by Newcome (*12*). Since then, alternative dendritic architectures and synthetic strategies have been proposed in the search of novel and improved properties (*13-16*).

Our group has recently reported on the preparation of dendrimers and their block copolymers with poly(ethylene glycol) (PEG), that incorporate a gallic acid-triethylene glycol repetition unit (GATG dendrimers) ([Gn]-$N_3$ and PEG-[Gn]-$N_3$, where n is the generation number, Scheme 1) (*17-20*). These structures are characterized by peripheral azides which facilitate their direct surface functionalization by means of the Cu(I)-catalyzed azide-alkyne cycloaddition (CuAAC) (*21*,*22*). Alternatively, reduction of the azides by hydrogenation or Staudinger reaction affords terminal amino groups which can be further elaborated by classical means (*e.g.*; amide or thiourea formation, reductive amination). The incorporation of the PEG chain in the block copolymers pursues to improve the biocompatibility, solubility, and biodistribution of the final conjugates (*23*,*24*). GATG dendrimers and block copolymers have emerged as promising tools for bioapplications, such as the study of the multivalent carbohydrate-receptor interaction (*25*) and the dynamics of glycodendrimers (*26*), or the preparation of drug and gene delivery nanosystems (*27*,*28*). More recently, GATG dendrimers have been also developed as contrast agents for MRI (*29*) and as inhibitors of the dimerization of the capsid protein of HIV-1 (*30*).

With the aim of further exploring the versatility of GATG dendrimers as tools in the biomedical field, in this work we exploit their easy click functionalization to synthesize a small library of dendrimers and PEG-dendritic block copolymers carrying different peripheral groups, and we evaluate their behavior in

living cells. Two series of dendritic systems were studied: one peripherally functionalized with charged/neutral groups having different physicochemical properties, and another one decorated with biologically relevant ligands such as, carbohydrates and peptides. Confocal microscopy was used to study the effect of functionalization on cell-uptake and intracellular trafficking, both properties of particular interest in drug delivery and other biomedical applications. Finally, this information was used to design a tailored carrier for the intracellular delivery and selective release of biologically active molecules. A PEG-dendritic copolymer carrying cargo molecules bound through a pH-sensitive linker was designed for selective cell uptake and release after lysosomal localization. The performance of this system was evaluated with a double fluorescent-labeling allowing for simultaneous monitoring the localization of the dendritic carrier and payload molecules.

**Experimental Section**

**Materials and methods.** $CuSO_4 \cdot 5H_2O$ and sodium bicarbonate were obtained from Prolabo. 4'-Ethynyl acetophenone and sodium ascorbate were purchased from Acros Organics. AMCA-hydrazide (AMCA, aminomethylcoumarin acetate) was purchased from Pierce Thermo Fisher Scientific. Triphenylphosphine and *t*-butanol were obtained from Sigma-Aldrich. $PEG_{5000}$-[G3]-$N_3$ (*17*) and [G3]-$N_3$ (*18*) were prepared following procedures previously described by our group. Alkynated fluorescein (FITC) (**1**) (*31*), sodium 3-butyn-1-sulfate (**2**) (*27*), and 2-propynyl β-D-lactopyranoside (**3**) (*18*) were prepared following reported procedures. Alkynated RDG peptide cyclo(RGDfPra) (**4**) was purchased from Peptide Synthetics. $H_2O$ was of Mili-Q grade. All other reagents were of analytical grade. Ultrafiltration was performed on Amicon stirred cells with Amicon YM3 membranes. NMR spectra were recorded on a Bruker DRX 500 MHz and Varian Mercury 300 MHz spectrometers. Chemical shifts are reported in ppm (δ units) downfield from internal tetramethylsilane ($CDCl_3$), the HOD solvent peak ($D_2O$) or residual solvent peak (DMSO-$d_6$). Resonances corresponding to FITC are only visible when spectra recorded in DMSO-$d_6$. UV-Vis spectra were performed on a HP 8452A Diode Array and

Jasco V-630 spectrophotometers. FT-IR spectra were recorded on a Bruker IFS-66v (neat samples, CsI window) or a Varian 670-IR equipped with a Varian 610-IR microscope.

**Synthesis and labeling**

**PEG-[G3]-FITC-$N_3$.** PEG-[G3]-$N_3$ (15 mg, 1.15 μmol) was dissolved in *t*-BuOH (0.16 mL) and $H_2O$ (0.12 mL). Then, alkynated FITC **1** (1.5 mg, 3.46 μmol) and freshly prepared aqueous solutions of $NaHCO_3$ (7 μL, 6.92 μmol, 1 M), $CuSO_4$ (14 μL, 0.69 μmol, 0.05 M), and sodium ascorbate (17 μL, 3.46 μmol, 0.2 M) were added. The resulting mixture was stirred at rt for 48 h, and then was purified by ultrafiltration ($H_2O$, 5 x 30 mL) to afford PEG-[G3]-FITC-$N_3$ (13.9 mg, 89%) as an orange foam. $^1$H NMR (500 MHz, DMSO-$d_6$) $\delta$: 8.54 (s, 1.2H), 8.50-8.39 (m, 10.8H), 7.25-7.10 (m, 26H), 4.50-3.93 (m, 82H), 3.88-3.43 (m, ~808H), 3.25 (s, 3H), 3.13-3.04 (m, 2H); (methylene protons adjacent to the azide groups are buried by the $H_2O$ signal). IR (KBr, cm$^{-1}$): 3278, 2871, 2106, 1112. UV-Vis ($H_2O$) $\lambda_{max}$: 296, 490 nm. UV-Vis (DMSO) $\lambda_{max}$: 520 nm. An average of 1.2 fluorescein molecules in PEG-[G3]-FITC-$N_3$ was determined by absorbance at 520 nm in DMSO, applying an extinction coefficient of 60800 M$^{-1}$ cm$^{-1}$. Same functionalization degree was obtained by integration of the triazol protons at 8.54 ppm in the $^1$H NMR (DMSO-$d_6$) spectrum.

**PEG-[G3]-FITC-$NH_3^+$.** $PPh_3$ (9.5 mg, 34.0 μmol) was added to a solution of PEG-[G3]-FITC-$N_3$ (13.9 mg, 1.03 μmol) in 2% $H_2O$/MeOH (1.0 mL). The resulting mixture was stirred at rt for 12 h. After addition of aqueous HCl (21 μL, 0.1 M), reaction was purified by ultrafiltration (50% MeOH/$H_2O$, 5 x 30 mL) to afford PEG-[G3]-FITC-$NH_2$·HCl (12.2 mg, 85%) as an orange foam. $^1$H NMR (500 MHz, $D_2O$) $\delta$: 7.21-7.08 (m, 26H), 4.32-4.07 (m, 80H), 3.98-3.50 (m, ~805H), 3.43 (s, 3H), 3.29-3.18 (m, 54H). IR (ICs window, MeOH, cm$^{-1}$): 2924, 1109. UV-Vis ($H_2O$) $\lambda_{max}$: 298, 490 nm. Peracetylation of this material with excess $Ac_2O$ in the presence of $Et_3N$ in MeOH (overnight, rt) afforded PEG-[G3]-FITC-NHAc after purification by extensive dialysis against $H_2O$ (MWCO 10 KDa).

**PEG-[G3]-FITC-$OSO_3^-$.** PEG-[G3]-FITC-$N_3$ (13.2 mg, 0.97 μmol) was dissolved in *t*-BuOH (0.13 mL) and $H_2O$ (0.07 mL). Then, sulfate **2** (9.1 mg, 52.6 μmol) and freshly prepared aqueous solutions of

$CuSO_4$ (26 μL, 1.32 μmol, 0.05 M) and sodium ascorbate (33 μL, 6.58 μmol, 0.2 M) were added. The resulting mixture was stirred at rt for 48 h, and then was purified by ultrafiltration ($H_2O$, 5 x 30 mL) to afford PEG-[G3]-FITC-$OSO_3Na$ (16.7mg, 95%) as an orange foam. $^1H$ NMR (500 MHz, $D_2O$) $\delta$: 8.14-7.83 (m, 27H), 7.30-7.00 (m, 26H), 4.62-4.50 (m, 54H), 4.47-4.01 (m, 132H), 4.00-3.49 (m, ~803H), 3.42 (s, 3H), 3.28-3.22 (m, 2H), 3.14-2.90 (m, 52H). IR (ICs window, neat, $cm^{-1}$): 3312, 2874, 1105. UV-Vis ($H_2O$) $\lambda_{max}$: 296, 490 nm.

**PEG-[G3]-FITC-Lac.** PEG-[G3]-FITC-$N_3$ (12.4 mg, 0.92 μmol) was dissolved in *t*-BuOH (0.12 mL) and $H_2O$ (0.07 mL). Then, lactoside **1** (19.6 mg, 49.4 μmol) and freshly prepared aqueous solutions of $CuSO_4$ (25 μL, 1.24 μmol, 0.05 M) and sodium ascorbate (31 μL, 6.18 μmol, 0.2 M) were added. The resulting mixture was stirred at 65 ºC for 60 h, and then was purified by ultrafiltration ($H_2O$, 5 x 30 mL) to afford PEG-[G3]-FITC-Lac (18.6 mg, 86%) as an orange foam. $^1H$ NMR (500 MHz, $D_2O$) $\delta$: 8.09-8.00 (m, 27H), 7.13-6.96 (m, 26H), 4.61-4.37 (m, 106H), 4.24-3.42 (m, ~1164H), 3.38 (s, 3H), 3.31-3.24 (m, 28H); (anomeric protons in lactose residues are buried by the HOD signal). IR (KBr, $cm^{-1}$): 3392, 2876, 1112. UV-Vis ($H_2O$) $\lambda_{max}$: 300, 490 nm.

**[G3]-FITC-Lac.** [G3]-$N_3$ (15 mg, 1.91 μmol) was dissolved in *t*-BuOH (0.26 mL) and $H_2O$ (0.19 mL). Then, alkynated FITC **1** (2.6 mg, 5.73 μmol) and freshly prepared aqueous solutions of $NaHCO_3$ (12 μL, 11.5 μmol, 1 M), $CuSO_4$ (23 μL, 1.15 μmol, 0.05 M), and sodium ascorbate (29 μL, 5.73 μmol, 0.2 M) were added. After 48 h of stirring at rt, lactoside **1** (40.9 mg, 0.103 mmol) and additional portions of $CuSO_4$ (14 μL, 1.43 μmol, 0.1 M) and sodium ascorbate (14 μL, 7.16 μmol, 0.5 M) were added. The resulting mixture was stirred at 65 ºC for 48 h, and then was purified by ultrafiltration ($H_2O$, 5 x 30 mL) to afford [G3]-FITC-Lac (27.3 mg, 77%) as an orange foam. $^1H$ NMR (500 MHz, $D_2O$) $\delta$: 8.20-7.97 (m, 27H), 7.25-6.85 (m, 26H), 4.94-4.85 (m, 26H), 4.76-4.69 (m, 26H), 4.61-4.38 (m, 106H), 4.18-3.39 (m, 700H), 3.36-3.27 (m, 26H), 3.26-3.19 (m, 2H), 1.60-1.45 (m, 2H), 0.94-0.81 (m, 3H). IR (KBr, $cm^{-1}$) 3418, 2925, 1077. UV-Vis ($H_2O$) $\lambda_{max}$: 262, 495 nm. UV-Vis (DMSO) $\lambda_{max}$: 520 nm. An average of 1.0 fluorescein molecules in [G3]-FITC-Lac was determined by absorbance at 502 nm in 50% DMSO/$H_2O$, applying an extinction coefficient of 61000 $M^{-1}$ $cm^{-1}$.

**PEG-[G3]-FITC-RGD.** PEG-[G3]-FITC-$N_3$ (2 mg, 0.15 μmol) was dissolved in *t*-BuOH (20 μL). Then, alkynated RGD peptide **4** (5.5 mg, 7.97 μmol) and freshly prepared aqueous solutions of $CuSO_4$ (10 μL, 0.20 μmol, 0.02 M) and sodium ascorbate (10 μL, 1.02 μmol, 0.1 M) were added. The resulting mixture was stirred at 65 ºC for 60 h, and then was purified by ultrafiltration [0.02 M EDTA (2 x 30 mL), $H_2O$ (2 x 30 mL), 0.01 M HCl (2 x 30 mL), $H_2O$ (5 x 30 mL)] to afford PEG-[G3]-FITC-RGD·HCl (3.6 mg, 84 %) as an orange foam. IR (ICs window, MeOH, $cm^{-1}$): 2866, 1582, 1496, 1109. UV-Vis ($H_2O$) $\lambda_{max}$: 234, 262, 502 nm.

**PEG-[G3]-AP-$N_3$.** PEG-[G3]-$N_3$ (36 mg, 2.77 μmol) was dissolved in *t*-BuOH (0.37 mL) and $H_2O$ (0.32 mL). Then, 4'-ethynyl acetophenone (0.8 mg, 5.53 μmol) and freshly prepared aqueous solutions of $CuSO_4$ (22 μL, 1.11 μmol, 0.05 M) and sodium ascorbate (28 μL, 5.53 μmol, 0.2 M) were added. The resulting mixture was stirred at rt for 48 h, and then was purified by ultrafiltration (50% MeOH/$H_2O$, 5 x 30 mL) to afford PEG-[G3]-AP-$N_3$ (36.1 mg, 98%) as a white foam. $^1$H NMR (500 MHz, $CDCl_3$) $\delta$: 8.27-8.02 (m, 1.4H), 8.00-7.69 (m, 5.6H), 7.22-7.01 (m, 26H), 4.68-4.47 (m, 2.8H), 4.46-3.96 (m, 80H), 3.95-3.44 (m, ~798), 3.42-3.21 (m, 56H), 2.58 (s, 2.1H), 2.54 (s, 2.1H). IR (KBr, $cm^{-1}$): 3438, 2874, 2108, 1113. An average of 1.4 acetophenone groups in PEG-[G3]-AP-$N_3$ was determined by integration of the characteristic aromatic signals of the acetophenone and dendritic scaffold in the $^1$H NMR spectrum in $CDCl_3$.

**PEG-[G3]-AP-FITC-$N_3$.** PEG-[G3]-AP-$N_3$ (18 mg, 1.37 μmol) was dissolved in *t*-BuOH (0.18 mL) and $H_2O$ (0.15 mL). Then, **1** (1.8 mg, 4.10 μmol) and freshly prepared aqueous solutions of $NaHCO_3$ (8 μL, 8.21 μmol, 1 M), $CuSO_4$ (16 μL, 0.82 μmol, 0.05 M), and sodium ascorbate (20 μL, 4.10 μmol, 0.2 M) were added. The resulting mixture was stirred at rt for 48 h, and then was purified by ultrafiltration ($H_2O$, 5 x 30 mL) to afford PEG-[G3]-AP-FITC-$N_3$ (16.2 mg, 87%) as an orange foam. $^1$H NMR (500 MHz, DMSO-$d_6$) $\delta$: 8.63 (s, 1.2H), 8.58 (s, 1.4H), 8.52-8.39 (m, 10.8H), 8.00-7.83 (m, 5.6H), 7.25-7.08 (m, 26H), 4.69-4.48 (m, 5.2H), 4.45-3.94 (m, 80H), 3.88-3.44 (m, ~805H), 3.25 (s, 3H), 3.13-3.04 (m, 2H); (methylene protons adjacent to the azide groups are buried by the $H_2O$ signal and methyl protons in acetophenone by residual DMSO). IR (KBr, $cm^{-1}$): 3381, 2873, 2106, 1116. UV-Vis ($H_2O$) $\lambda_{max}$: 296,

495 nm. UV-Vis (DMSO) $\lambda_{max}$: 520 nm. An average of 1.2 fluorescein molecules in PEG-[G3]-AP-FITC-$N_3$ was determined by absorbance at 520 nm in DMSO, applying an extinction coefficient of 60800 $M^{-1}$ $cm^{-1}$.

**PEG-[G3]-AMCA-FITC-$N_3$.** PEG-[G3]-AP-FITC-$N_3$ (16.2 mg, 1.18 μmol) and AMCA-hydrazide (2.5 mg, 10.1 μmol, 620 mol% per ketone) were dissolved in DMF (0.12 mL). Then, a pyridine/acetic acid mixture (3:1, 120 μL) was added. The resulting solution was stirred at rt for 48 h, and then it was concentrated and purified by ultrafiltration (50% MeOH/$H_2O$, 5 x 30 mL) to afford PEG-[G3]-AMCA-FITC-$N_3$ (16.1 mg, 97%) as a yellow foam. $^1$H NMR (500 MHz, $CDCl_3$) $\delta$: 8.22-8.05 (m, 1.4H), 7.98-7.77 (m, 5.6H), 7.27-6.91 (m, 26H), 4.63-4.38 (m, 2.8H), 4.26-3.95 (m, 80H), 3.93-3.50 (m, ~800H), 3.36-3.17 (m, 54H), 2.61-2.45 (m, 4.2H); (because of their low intensity, AMCA signals are not included). UV-Vis ($H_2O$) $\lambda_{max}$: 298, 350, 496 nm.

**PEG-[G3]-AMCA-FITC-$NH_2$.** $PPh_3$ (10.0 mg, 38.4 μmol) was added to a solution of PEG-[G3]-AMCA-FITC-$N_3$ (16.1 mg, 1.15 μmol) in 2% $H_2O$/MeOH (1.1 mL). The resulting mixture was stirred at rt for 12 h, and then it was purified by ultrafiltration (50% MeOH/$H_2O$, 5 x 30 mL) to afford PEG-[G3]-AMCA-FITC-$NH_2$ (14.7 mg, 95%) as a yellow foam. IR (ICs window, $CHCl_3$, $cm^{-1}$): 3270, 2870, 1107. UV-Vis ($H_2O$) $\lambda_{max}$: 302, 350, 500 nm. An average of 1.0 AMCA in PEG-[G3]-AMCA-FITC-$NH_2$ was determined by measuring the increase in absorbance at 350 nm in $H_2O$ with respect to PEG-[G3]-AP-FITC-$N_3$, applying an extinction coefficient of 19000 $M^{-1}$ $cm^{-1}$.

**Cell Culture.** HeLa, MCF7, and HepG2 cells were purchased from ATCC and cultured following manifacturer's instructions. For live cell microscopy, cells were plated onto 35 mm glass-bottom dishes (WillCo-dish GWSt-3522) and imaged at 37 ºC, 5% $CO_2$.

**Confocal Imaging.** Cell imaging was performed on a Leica TCS SP2 inverted confocal microscope (Leica Microsystems) equipped with a 40 × 1.25 NA oil immersion objective (Leica Microsystems). Imaging was obtained illuminating the samples with the inline Ar and He-Ne lasers of the microscope and with a 403 nm pulsed diode laser (M8903-01; Hamamatsu) at 50 MHz repetition rate. Fluorescence emission was collected with the AOBS-based built-in detectors of the confocal microscope (Hamamatsu

R6357). Nuclei were stained with Hoechst and imaged using the 403nm laser. Simultaneous AMCA and fluorescein imaging was performed by means of a Leica AF6000 wide-field setup.

**Propidium Iodide (PI) Assay.** HeLa cells were incubated for 2 h at 37 ºC with DMEM (Dulbecco's Modified Eagle Medium) containing 8 $\mu$g/mL propidium iodide and different concentrations of dendrimer. The medium was then discarded and cells were washed with PBS buffer containing the same concentration of propidium iodide before confocal imaging.

**Flow Cytometry Measurements.** Cells were grown in a six well plate and after treatment with labeled dendrimer were detached using trypsin-EDTA, washed with PBS buffer and fixed with 4% paraformaldheyde (PFA). Cells were washed with PBS until complete removal of PFA and finally resuspended in 250 $\mu$L of PBS. Flow cytometry was performed on a FACScalibur system (BD biosciences) by counting 10000 events. Histogram plots were analyzed using WinMDI 2.9 (http://facs.scripps.edu/software.html).

**Toxicity Assay.** HeLa cells were incubated for 1 h at 37 °C with DMEM containing 8 $\mu$g/mL propidium iodide and different concentrations of dendrimer. The medium was then discarded and the cells were washed with PBS buffer three times. Calcein-AM was then added and incubated for 15 min before confocal imaging.

**Internalization Assay and Colocalization Studies.** To monitor dendrimer internalization, cells were incubated with 100 nM fluorescein-labeled dendrimers in DMEM for 1 h at 37 ºC. To remove unbound molecules in the medium, cells were rinsed twice with PBS. After the initial preloading and subsequent washing, cells were incubated again in DMEM and imaged at the indicated time point. In order to identify the endocytic vesicles involved in dendrimer internalization, colocalization assays were performed in living cells. HeLa cells were coincubated with dendrimers (as described above) and different dyes: 1 mg/mL of a 70 KDa dextran-TRITC conjugate at 37 ºC for 30 min to label macropinosomes, 50 mM Lysotracker for 10 min to label lysosomes, and 2 $\mu$g/mL of a transferrin-Alexa568 conjugate to label clathrin-coated endosomes. Images were analyzed using ImageJ software version 1.37 (NIH Image; http://rsbweb.nih.gov/ij).

**Results and Discussion**

With the aim of analysing the effect of the peripheral substitution of GATG dendrimers on their uptake and intracellular trafficking in living cells, biologically relevant ligands and groups with different physicochemical properties were selected to functionalize the surface of a dendrimer and a $PEG_{5000}$-dendritic block copolymer of G3 ([G3]-$N_3$ and PEG-[G3]-$N_3$) (Scheme 1). The 27 peripheral azides on these structures provide a large degree of multivalency for the easy incorporation of several tags and ligands, and for a subsequent effective interaction with cell surfaces. To this end, a common synthetic strategy was followed that involved an initial functionalization of PEG-[G3]-$N_3$ and [G3]-$N_3$ with the alkynated FITC derivative **1** by CuAAC ($CuSO_4$, sodium ascorbate, *t*-BuOH-$H_2O$) in excellent yields (Scheme 1). The incorporation of one FITC molecule on average, determined by absorbance and NMR, resulted in dendritic structures that can be monitored by confocal microscopy. Decoration of the remaining azides with cationic/neutral/anionic groups or biologically relevant ligands, such as carbohydrates and peptides, afforded a small library of dendritic structures as tools to evaluate the effect of peripheral groups on the cell-uptake and intracellular trafficking of GATG dendrimers (Scheme 1).

To this end, anionic sulfate residues were easily introduced on the block copolymer by CuAAC (**2**, $CuSO_4$, sodium ascorbate, *t*-BuOH-$H_2O$) to give PEG-[G3]-FITC-$OSO_3^-$ in 95% yield. Cationic and neutral groups were incorporated *via* Staudinger reaction ($PPh_3$, $H_2O$-MeOH) and subsequent acetylation to afford respectively PEG-[G3]-FITC-$NH_3^+$·and PEG-[G3]-FITC-NHAc in excellent yields. In a similar way, the biologically relevant carbohydrate and peptide ligands, lactose and RGD, were introduced by CuAAC (**3** or **4**, $CuSO_4$, sodium ascorbate, *t*-BuOH-$H_2O$) leading to [G3]-FITC-Lac, PEG-[G3]-FITC-Lac, and PEG-[G3]-FITC-RGD in excellent yields. Complete functionalization of peripheral azides in all these conjugates was confirmed by $^1H$ NMR ($D_2O$) by disappearance of the characteristic signal of the methylene protons adjacent to the azide groups (3.40 ppm). IR spectroscopy additionally confirmed complete functionalization by disappearance of the intense azide signal at around 2100 $cm^{-1}$.

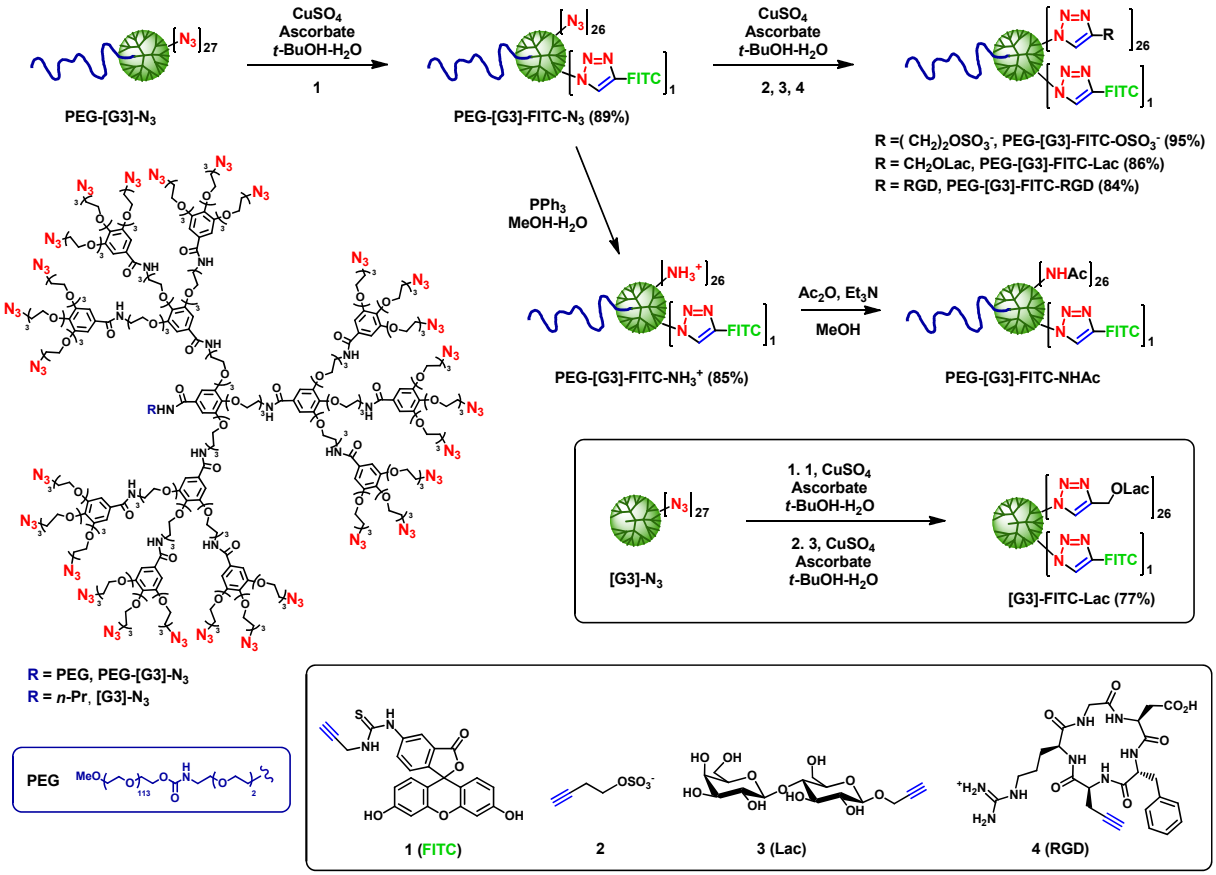


**Scheme 1**

### Peripheral functionalization of PEG-GATG regulates cell uptake

To address the ability of PEG-GATG block copolymers to cross the plasma membrane and to be internalized into living cells, we studied their interactions with cultured HeLa cells by confocal microscopy as a function of the physicochemical properties (charge and hydrophobicity) on their surface. In particular, we initially focused our attention on three surface groups: i) primary amines (PEG-[G3]-FITC-$NH_3^+$), ii) acetylated amines (PEG-[G3]-FITC-NHAc), and iii) sulfate groups (PEG-[G3]-FITC-$OSO_3^-$), which display cationic, neutral, and anionic character at physiological pH, respectively.

Figure 1 shows confocal images of HeLa cells treated with these three groups of FITC-labeled structures. A strong effect of the surface charge on cell uptake was observed in agreement with previous reports with alternative dendritic families (*32*,*33*). While cationic PEG-[G3]-FITC-$NH_3^+$ showed a

strong internalization consistent with its ability to bind cell membranes through ionic interactions, anionic PEG-[G3]-FITC-$OSO_3^-$ showed only a weak internalization because of its lower affinity for cell membranes. This behavior is even more evident for neutral PEG-[G3]-FITC-NHAc, showing no internalization at all in HeLa cells. A strong difference between cationic and anionic dendritic structures has been also observed in the kinetics of internalization (see Figure S1 in the Supporting Information). Thus, PEG-[G3]-FITC-$NH_3^+$ showed a long residence time on the plasma membrane and slow internalization, while no accumulation on the membrane and fast internalization (perinuclear localization after 1 h) was observed for the anionic counterpart. This observed relationship between charge and internalization efficiency is of great interest for the application of these materials in nanomedicine, as it would allow controlling the behavior of dendritic carriers by selecting the physicochemical properties on their surface.

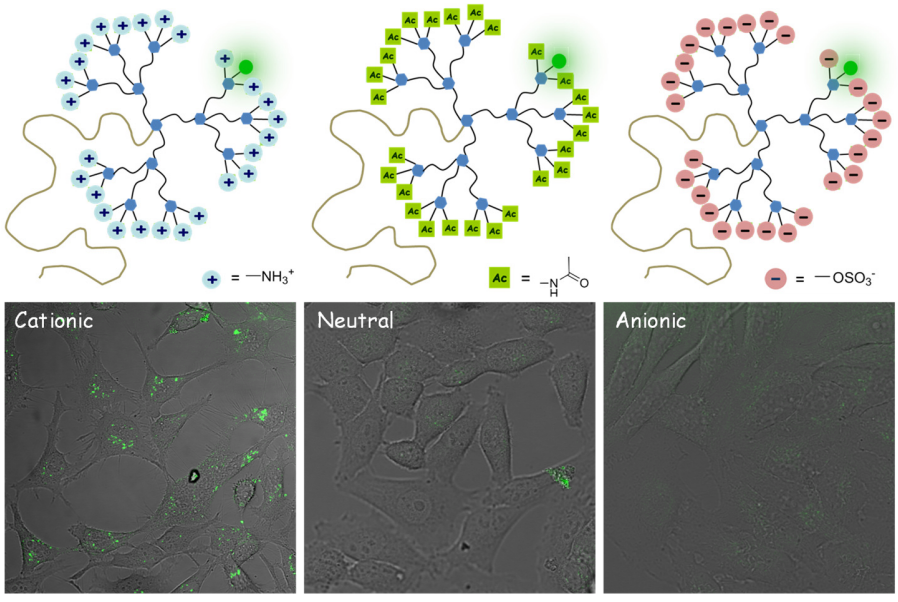


**Figure 1.** Confocal images of HeLa cells treated with PEG-GATG copolymers carrying different surface charge. Cells were incubated with labeled dendrimers for 1 h, and then were washed with PBS and imaged after 8 h.

Further studies with the most internalizing derivative, PEG-[G3]-FITC-$NH_3^+$, were performed to unveil the details of its uptake properties. Figure 2a shows a time lapse imaging of this copolymer where three main phases of internalization can be observed: i) membrane binding, ii) formation of intracellular

vesicles, and iii) delivery to the perinuclear region. These results are in good agreement with previous observations with PAMAM dendrimers and suggest endocytosis as the main way of entrance for these macromolecules inside cells. Next, we decided to investigate the mechanism of cell uptake by means of colocalization assays using red-labeled endocytic markers (Figure 2b). After 4 h of administration, a good colocalization of PEG-[G3]-FITC-$NH_3^+$ (100 nM) was observed with a 70 KDa dextran, a specific marker of macropinocytosis. In contrast, no colocalization was observed with transferrin, indicating that the copolymer does not localize in clathrin-coated vesicles. This result slightly differs from previous observations with PAMAM dendrimers that showed a prevalence of macropinocytosis accompanied by a significant population of dendrimers entering cells through a clathrin-mediated pathway. In general, macropinocytosis is the preferred pathway for non-specific cell binding and although it converges with the clathrin pathway at a later stage, some significant differences between both exist; in particular the kinetic of internalization for macropinocytosis is usually slower. Further studies of colocalization with endocytic markers and inhibitors of the different pathways will be of help to confirm these results.

Moreover, the final fate of PEG-[G3]-FITC-$NH_3^+$ trafficking in HeLa cells was identified (Figure 2b). Colocalization with lysotroacker, a well-known lysosome marker, clearly showed the copolymer fully localizing in the lysosomes after 12 h, a fact which is considered of great interest for drug delivery applications as lysosomes are endowed with a peculiar chemical environment (low pH, high ionic strenght and abundance of hydrolytic enzymes). As shown below, advantage was taken of these internalization properties for the design of a drug delivery system with the ability to trigger the release of drugs.

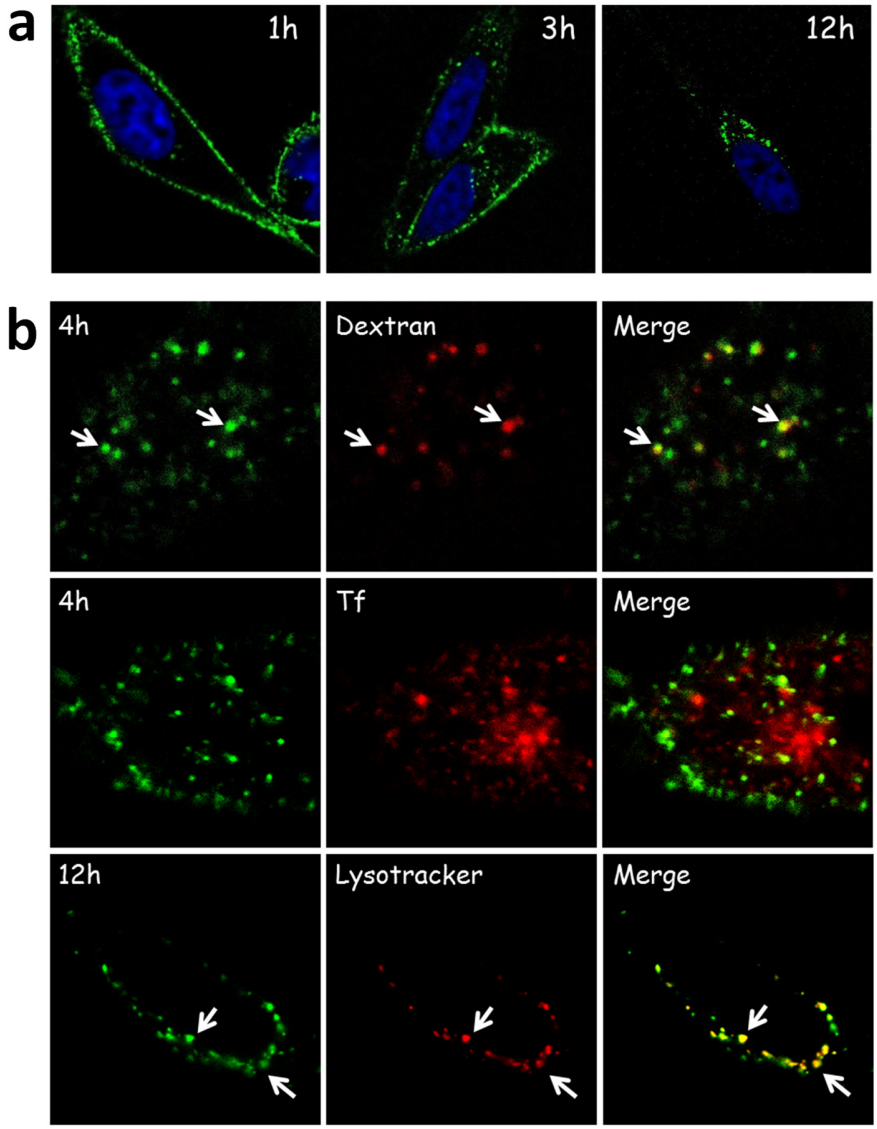


**Figure. 2.** (a) Time lapse imaging of PEG-[G3]-FITC-$NH_3^+$ (green) in HeLa cells and (b) colocalization assays with different endocytic markers (red): dextran for macropinocytosis (top), transferrin for clathrin pathway (middle), and lysotracker (bottom).

**Concentration-dependent uptake mechanism**

Internalization studies with PEG-[G3]-FITC-$NH_3^+$ were performed in HeLa cells that shed light on the concentration-dependence of the process. Figure 3 shows the cellular localization of the copolymer at different concentrations after 15 min of incubation. At concentrations up to 1 μM, PEG-[G3]-FITC-$NH_3^+$ showed membrane binding as previously described. However, at higher concentrations, a

completely different localization pattern appeared with copolymers widely spread in the cytoplasm and accumulated into the nucleoli. This localization suggested the possibility of a direct membrane translocation mechanism in agreement with previous reports by Holl and coworkers on the ability of PAMAM dendrimers of high generations (from G7) to create temporary holes in the plasma membrane (*34*). To confirm this mechanism in our case, a propidium iodide assay was performed that revealed an altered permeability of the cell membrane for PEG-[G3]-FITC-$NH_3^+$ at a concentration 10 μM. It is interesting to note that while this phenomenon operates in PEG-GATG copolymers of G3 with only 27 amines, an order of magnitude higher in peripheral amines is required for PAMAM dendrimers to alter cell membranes. This difference could be related to the higher flexibility of the GATG dendritic scaffold which may exploit more efficiently the peripheral cationic groups as ionic binders. Interestingly, the observed nucleolar localization is in good agreement with previously reported intracellular studies with cationic PAMAM dendrimers (*35*).

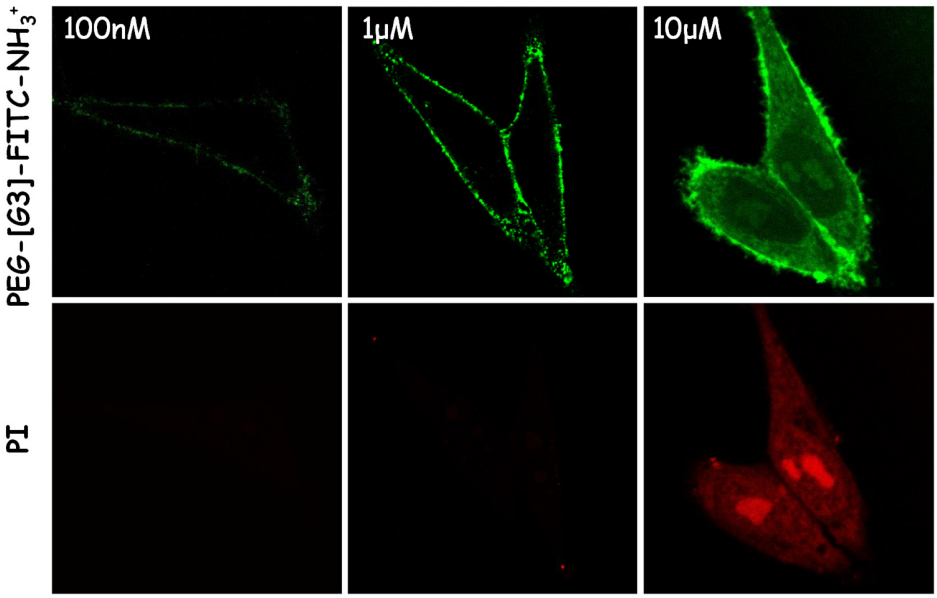


**Figure. 3.** Localization of FITC-labeled cationic PEG-[G3]-FITC-$NH_3^+$ in HeLa cells after 15 min at different concentrations (top). Cells were treated with the copolymer in the presence of propidium iodide (bottom) to study the membrane permeability during treatment.

**Carbohydrate-decorated copolymers**

Carbohydrates regulate a plethora of biological and pathological processes in Nature. Recognition events such as fertilization, toxin and hormone mediation, pathogen invasion, and cell-cell interactions rely on multivalent carbohydrate-receptor interactions (*36*-*38*). This cluster glycoside effect has prompted the development of glycodendrimers with the ability to interact with target lectins and to promote/inhibit natural carbohydrate-receptor interactions (*25*,*39*). In this context, an approach of our laboratory to speed up the preparation of glycodendrimers has taken advantage of the chemical compatibility of unprotected carbohydrates with the typical reaction conditions of CuAAC. This way, not only subsequent deprotection reactions are avoided, but also functionalization facilitated by reduced steric hindrance (*17*,*18*).

Lactose (Lac) represents an especially attractive carbohydrate of low molecular weight. Thanks to its high biocompatibility and ability to target specific cell populations, Lac has been already proposed as coating agent for dendrimers with potential applications in antiadhesive therapy (*40*) and drug delivery toward hepatocytes (*41*). Focusing our attention on this latter application, HepG2 cells derived from hepatocarcinoma and endowed with the asialoglycoprotein receptor (ASGPR, that can recognize and internalize lactose moieties) were incubated with lactose-decorated PEG-[G3]-FITC-Lac (Figure 4). [G3]-FITC-Lac was also included in this study to investigate the influence of PEG on the ability of GATG dendrimers to interact with cell surfaces. Confocal microscopy revealed that both structures were taken up by cells, but with very different efficacy. Indeed, it is evident from Figure 4 that PEG-[G3]-FITC-Lac is much less internalized by HepG2 cells compared to the non-PEGylated dendrimer, a difference that might arise from the ability of PEG to shield lactose ligands and hence, limit cell-dendrimer interactions. Notably, when experiments were performed in the presence of an excess of free lactose (up to 150 mM), internalization revealed unaffected. In the same way, comparable levels of internalization were observed with HeLa cells, indicating that receptor-mediated endocytosis is not the only pathway of internalization in the case of these dendrimers. Based on this significant cell-uptake and

the known biocompatibility associated to carbohydrates, we believe these carbohydrate-coated dendrimers deserve further investigation as tools for cell internalization as alternative to classical cationic dendrimers, while avoiding the characteristic higher toxicity of the latter (Figure S2).

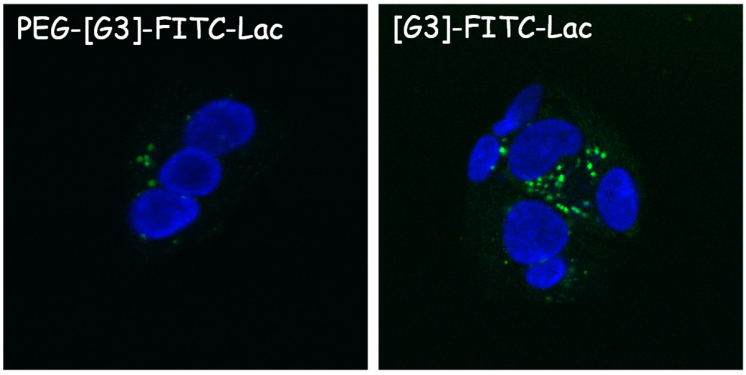


**Figure 4.** Localization of PEG-[G3]-FITC-Lac (left) and [G3]-FITC-Lac (right) after 2 h incubation with HepG2 cells.

**Peptide-decorated copolymers**

Peptides are common targeting vectors in nanobiotechnology thanks to their small size, easy large-scale synthesis, and retained activity upon conjugation. Solid-phase synthesis of peptides allows their easy modification with chemical handles for incorporation into nanostructures. In this work we report the synthesis and biological evaluation of a peptide-decorated PEG-[G3]-FITC-RGD which incorporates multiple copies of a cyclic RGD (Arg-Gly-Asp) peptide. RGD peptides are of great interest for their ability to be effectively recognized by integrins. These are heterodimeric cell-surface proteins that play important roles in cell adhesion and signalling (*42*), and are overexpressed in pathologies such as cancer and atherosclerosis (*43*). The clustered arrangement of integrins on cell surfaces has stimulated the preparation of RGD-coated dendrimers for enhanced affinity through multivalent interactions (*44*). The alkynated cyclo(RGDfPra) peptide **4** incorporated in PEG-[G3]-FITC-RGD is a mimetic of Cilengitide, a peptide with superior integrin binding affinity, currently under clinical trials in patients with glioblastoma (*45-47*).

Figure 5 shows the internalization efficacy of PEG-[G3]-FITC-RGD in two cell lines: HeLa cells that overexpress the αvβ3 integrin, and MCF7 which are reported to have low expression level of this membrane protein. Both confocal imaging and flow cytometry show a strong internalization in HeLa cells, but a response comparable to a negative control in MCF7 cells. Clearly, the presence of RGD peptides on the surface of PEG-[G3]-FITC-RGD grants the whole nanostructure with targeting and internalization properties to specific cell populations. These results along with the modular synthetic approach and easy functionalization of GATG dendrimers reveal PEG-[G3]-FITC-RGD as a prototype of a family of peptide-driven targeted nanostructures with promising biological applications.

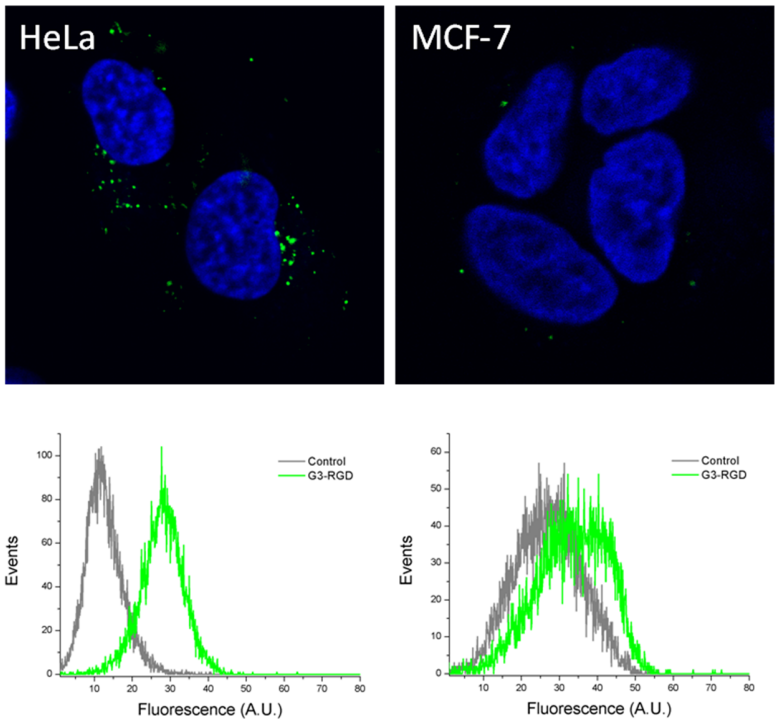


**Figure 5.** (a) Localization of PEG-[G3]-FITC-RGD in HeLa cells (left) and MCF7 (right). (b) Flow cytometry quantification of cell uptake in the two cell lines.

**Development of a dendritic pH-sensitive drug delivery system for selective release after lysosomal localization**

The possibility of delivering nanostructures to specific cell compartments with particular biochemical environments (pH, ionic strength, enzymatic activity) is of crucial interest for drug delivery applications

(*48*). Lysosomes are especially interesting in this context as their characteristic acidic pH (usually below 5.0) can be exploited to trigger the release of active species inside cells (*49*). In the previous sections we have demonstrated the internalization mechanism of PEG-[G3]-FITC-$NH_3^+$ through macropinocytosis and its final delivery to the lysosomal compartment. In this section, we describe a drug delivery prototype that based on this structure exploits pH-cleavable hydrazone linkers (stable at physiological pH but hydrolysable under acidic media) for the selective delivery of cargo molecules inside cells (Scheme 2). With the aim of simultaneously monitoring the localization of the dendritic carrier and payload molecules in this system, a dual fluorescent-labeling strategy was pursued combining FITC and a coumarin dye (AMCA-Hydrazide) as model cargo molecule (Scheme 2).

For the preparation of this delivery system, an ethynyl acetophenone linker (**AP**) was first introduced by CuAAC into PEG-[G3]-$N_3$ as a chemical handle for subsequent hydrazone formation ($CuSO_4$, sodium ascorbate, *t*-BuOH-$H_2O$, 98% yield). The resulting PEG-[G3]-AP-$N_3$ conjugate carrying one acetophenone on average (as determined by NMR) was then tagged by CuAAC with a FITC dye (**1**, $NaHCO_3$, $CuSO_4$, sodium ascorbate, *t*-BuOH-$H_2O$). PEG-[G3]-AP-FITC-$N_3$ was obtained in 87% yield with an average of one FITC as determined by absorbance. The appearance of two singlets at 8.63 and 8.58 ppm corresponding to two triazol protons in the $^1$H NMR spectrum of PEG-[G3]-AP-FITC-$N_3$ confirms the dual CuAAC labeling. Incorporation of AMCA-Hydrazide at this stage was followed by reduction of the remaining azides *via* Staudinger conditions to afford the desired PEG-[G3]-AMCA-FITC-$NH_2$ in excellent overall yield. Complete functionalization/reduction of peripheral azides in this system was confirmed by disappearance of the intense azide signal at around 2100 $cm^{-1}$ in the IR spectrum.

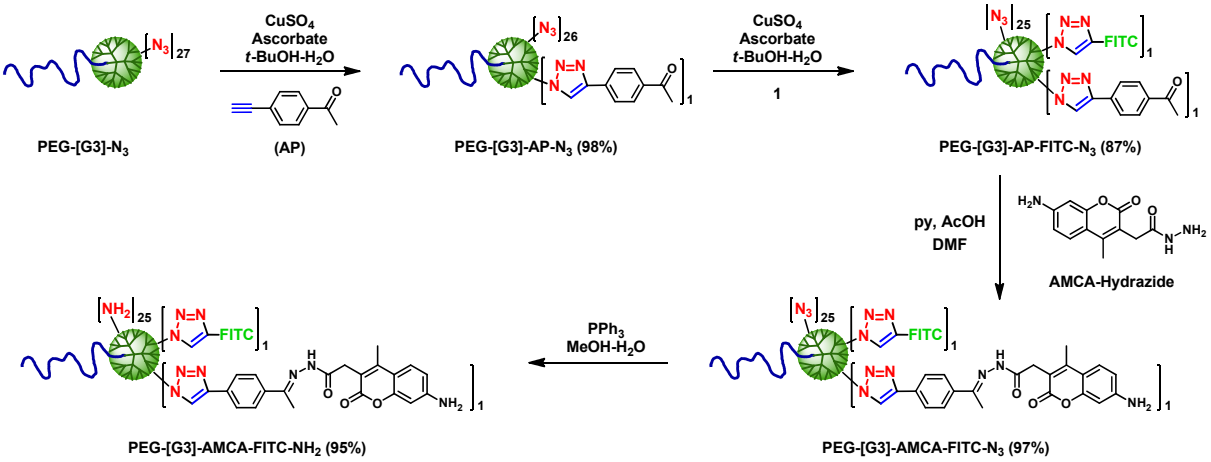


**Scheme 2**

Fluorescence experiments with PEG-[G3]-AMCA-FITC-$NH_2$ were performed in HeLa cells over a period of 18 h (Figure 6). At short incubation times, high colocalization between FITC and AMCA was seen in the endolysosomal system in agreement with the integrity of the conjugate. The low fluorescence intensity of AMCA at this stage is probably due to a probe–probe quenching effect. At longer incubation times, two main phenomena revealed in dendrimer-treated cells: i) an increase in the fluorescence intensity of AMCA; and ii) a reduced colocalization of AMCA and FITC. These observations have been interpreted as resulting from hydrolysis of the hydrazone linkers at the lysosome and release of the AMCA molecules. Moreover, as AMCA seems to be localized in the cytoplasm, this suggests the ability of this small and hydrophobic dye to escape the endosome, while the hydrophilic and bulky dendrimer prevents the endosomal escape of the covalently attached fluorescein. Accordingly, this GATG-based conjugate is able to accomplish the main requirements for a successful drug delivery system: cell internalization, intracellular release, and endosome escaping. This promising proof of principle opens the way for the application of GATG dendrimers for specific issues in pharmacology.

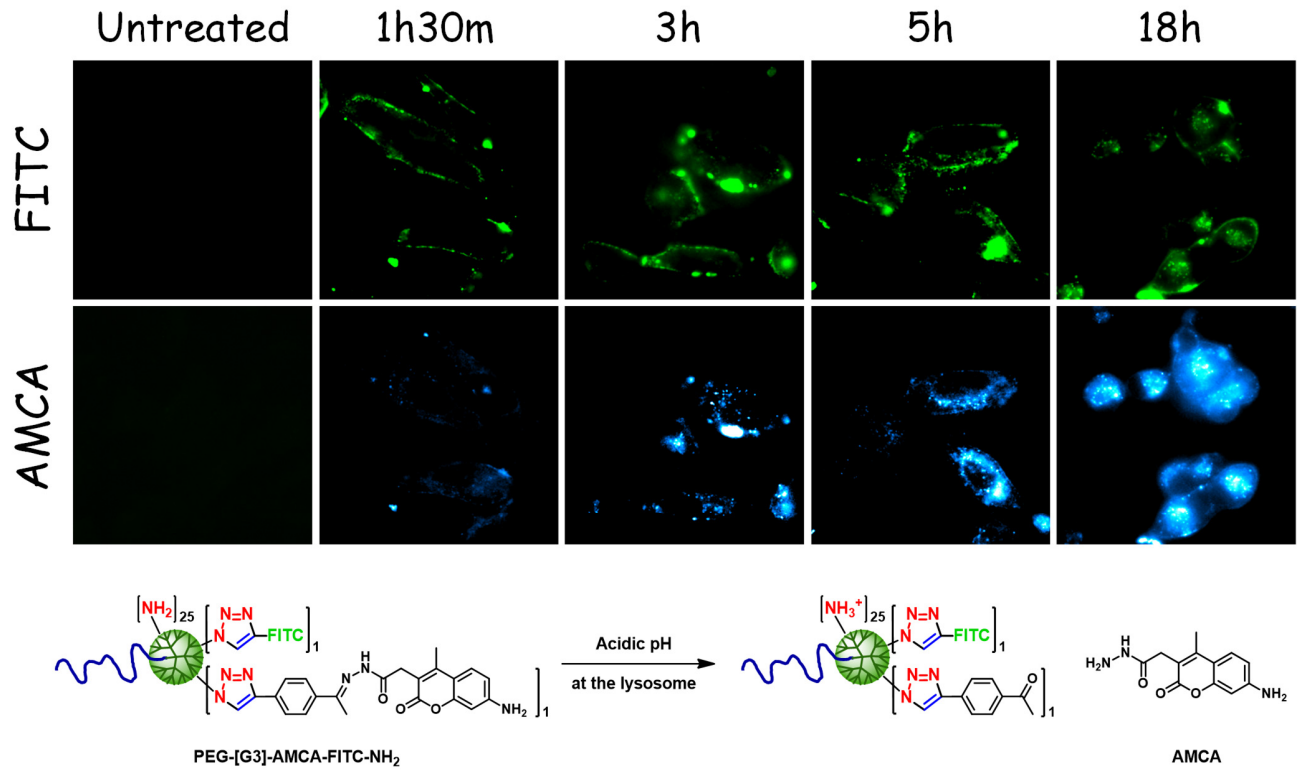


**Figure 6.** HeLa cells treated for 18 h with PEG-[G3]-AMCA-FITC-$NH_2$. Fluorescent signals from fluorescein (top panels) and AMCA (bottom panels) were recorded at different times.

## Conclusions

In this paper we exploit the versatility of GATG dendrimers to obtain a wide array of surface functionality. The interaction of these materials with cells has been studied by confocal microscopy, unveiling a strong relationship between peripheral decoration at the dendrimer and relevant properties for their bioapplications, such as cell internalization and localization. This information has been exploited to design a drug delivery vector able to intracellularly release a model compound. These results disclose relevant insights about the behavior of GATG dendrimers in the biological environment and represent an important step toward their use for clinical purposes.

**Acknowledgment.** This work was financially supported by the Spanish MICINN (CTQ2009-10963 and CTQ2009-14146-C02-02) and the Xunta de Galicia (10CSA209021PR and CN2011/037). M.F.-V. thanks the Spanish Ministry of Education for a FPU fellowship.

**References**

(1) Menjoge, A. R., Kannan, R. M., and Tomalia, D. A. (2010) Dendrimer-based drug and imaging conjugates: design considerations for nanomedical applications. *Drug Discov. Today 15*, 171-185.

(2) Gillies, E. R., and Fréchet, J. M. J. (2005) Dendrimers and dendritic polymers in drug delivery. *Drug Discov. Today 10*, 35-43.

(3) Lee, C. C., MacKay, J. A., Fréchet, J. M. J., and Szoka, F. C. (2005) Designing dendrimers for biological applications. *Nat. Biotechnol. 23*, 1517-1526.

(4) Shcharbin, D., Pedziwiatr, E., Blasiak, J., and Bryszewska, M. (2010) How to study dendriplexes II: Transfection and cytotoxicity. *J. Controlled Release 141*, 110-127.

(5) Rolland, O., Turrin, C.-O., Caminade, A.-M., and Majoral, J.-P. (2009) Dendrimers and nanomedicine: multivalency in action. *New J. Chem. 33*, 1809-1824.

(6) Tekade, R. K., Kumar, P. V., and Jain, N. K. (2009) Dendrimers in Oncology: An Expanding Horizon. *Chem. Rev. 109*, 49-87.

(7) Villaraza, A. J. L., Bumb, A., and Brechbiel, M. W. (2010) Macromolecules, Dendrimers, and Nanomaterials in Magnetic Resonance Imaging: The Interplay between Size, Function, and Pharmacokinetics. *Chem. Rev. 110*, 2921-2959.

(8) Sakadžić, S., Roussakis, E., Yaseen, M. A., Mandeville, E. T., Srinivasan, V. J., Arai, K., Ruvinskaya, S., Devor, A., Lo, E. H., Vinogradov, S. A., and Boas, D. A. (2010) Two-photon high-

resolution measurement of partial pressure of oxygen in cerebral vasculature and tissue. *Nat. Methods 7*, 755-759.

(9) Albertazzi, L., Brondi, M., Pavan, G. M., Sato, S. S., Signore, G., Storti, B., Ratto, G. M., and Beltram, F. (2011) Dendrimer-Based Fluorescent Indicators: In Vitro and In Vivo Applications. *PLoS ONE 6*, e28450.

(10) Buhleier, E., Wehner, W., and Vögtle, F. (1978) "Cascade"- and "Nonskid-Chain-like" Syntheses of Molecular Cavity Topologies. *Synthesis*, 155-158.

(11) Tomalia, D. A., Baker, H., Dewald, J., Hall, M., Kallos, G., Martin, S., Roeck, J., Ryder, J., and Smith, P. (1985) A New Class of Polymers: Starburst-Dendritic Macromolecules. *Polym. J. 17*, 117-132.

(12) Newkome, G. R., Yao, Z.-q., Baker, G. R., and Gupta, V. K. (1985) Cascade molecules: a new approach to micelles. A [27]-arborol. *J. Org. Chem. 50*, 2003-2004.

(13) Hawker, C. J., and Fréchet, J. M. J. (1990) Preparation of polymers with controlled molecular architecture. A new convergent approach to dendritic macromolecules. *J. Am. Chem. Soc. 112*, 7638-7647.

(14) Astruc, D., Boisselier, E., and Ornelas, C. (2010) Dendrimers Designed for Functions: From Physical, Photophysical, and Supramolecular Properties to Applications in Sensing, Catalysis, Molecular Electronics, Photonics, and Nanomedicine. *Chem. Rev. 110*, 1857-1959.

(15) Vögtle, F., Richardt, G., and Werner, N. *Dendrimer Chemistry*; Wiley-VCH: Weinheim, 2009.

(16) *Dendrimers and Other Dendritic Polymers*; John Wiley & Sons, Ltd.: Chichester, 2001.

(17) Fernandez-Megia, E., Correa, J., and Riguera, R. (2006) "Clickable" PEG-Dendritic Block Copolymers. *Biomacromolecules 7*, 3104-3111.

(18) Fernandez-Megia, E., Correa, J., Rodríguez-Meizoso, I., and Riguera, R. (2006) A Click Approach to Unprotected Glycodendrimers. *Macromolecules 39*, 2113-2120.

(19) Amaral, S. P., Fernandez-Villamarin, M., Correa, J., Riguera, R., and Fernandez-Megia, E. (2011) Efficient Multigram Synthesis of the Repeating Unit of Gallic Acid-Triethylene Glycol Dendrimers. *Org. Lett. 13*, 4522-4525.

(20) Meunier, S. J., Wu, Q., Wang, S.-N., and Roy, R. (1997) Synthesis of hyperbranched glycodendrimers incorporating α-thiosialosides based on a gallic acid core. *Can. J. Chem. 75*, 1472–1482.

(21) Tornøe, C. W., Christensen, C., and Meldal, M. (2002) Peptidotriazoles on Solid Phase: [1,2,3]-Triazoles by Regiospecific Copper(I)-Catalyzed 1,3-Dipolar Cycloadditions of Terminal Alkynes to Azides. *J. Org. Chem. 67*, 3057-3064.

(22) Rostovtsev, V. V., Green, L. G., Fokin, V. V., and Sharpless, K. B. (2002) A Stepwise Huisgen Cycloaddition Process: Copper(I)-Catalyzed Regioselective "Ligation" of Azides and Terminal Alkynes. *Angew. Chem., Int. Ed. 41*, 2596-2599.

(23) Harris, J. M., and Chess, R. B. (2003) Effect of pegylation on pharmaceuticals. *Nat. Rev. Drug Discov. 2*, 214-221.

(24) Joralemon, M. J., McRae, S., and Emrick, T. (2010) PEGylated polymers for medicine: from conjugation to self-assembled systems. *Chem. Commun. 46*, 1377-1393.

(25) Munoz, E. M., Correa, J., Fernandez-Megia, E., and Riguera, R. (2009) Probing the Relevance of Lectin Clustering for the Reliable Evaluation of Multivalent Carbohydrate Recognition. *J. Am. Chem. Soc. 131*, 17765-17767.

(26) Novoa-Carballal, R., Säwén, E., Fernandez-Megia, E., Correa, J., Riguera, R., and Widmalm, G. (2010) The dynamics of GATG glycodendrimers by NMR diffusion and quantitative 13C relaxation. *Phys. Chem. Chem. Phys. 12*, 6587-6589.

(27) Sousa-Herves, A., Fernandez-Megia, E., and Riguera, R. (2008) Synthesis and supramolecular assembly of clicked anionic dendritic polymers into polyion complex micelles. *Chem. Commun.*, 3136-3138.

(28) Raviña, M., de la Fuente, M., Correa, J., Sousa-Herves, A., Pinto, J., Fernandez-Megia, E., Riguera, R., Sanchez, A., and Alonso, M. J. (2010) Core−Shell Dendriplexes with Sterically Induced Stoichiometry for Gene Delivery. *Macromolecules 43*, 6953-6961.

(29) Fernández-Trillo, F., Pacheco-Torres, J., Correa, J., Ballesteros, P., Lopez-Larrubia, P., Cerdán, S., Riguera, R., and Fernandez-Megia, E. (2011) Dendritic MRI Contrast Agents: An Efficient Prelabeling Approach Based on CuAAC. *Biomacromolecules 12*, 2902-2907.

(30) Doménech, R., Abian, O., Bocanegra, R., Correa, J., Sousa-Herves, A., Riguera, R., Mateu, M. G., Fernandez-Megia, E., Velázquez-Campoy, A., and Neira, J. L. (2010) Dendrimers as Potential Inhibitors of the Dimerization of the Capsid Protein of HIV-1. *Biomacromolecules 11*, 2069-2078.

(31) Ikeda, M., Minari, J., Shimada, N., Numata, M., Sakurai, K., and Shinkai, S. (2007) Complex formation between cationic □-1,3-glucan and hetero-sequence oligodeoxynucleotide and its delivery into macrophage-like cells to induce cytokine secretion. *Org. Biomol. Chem. 5*, 2219-2224.

(32) Perumal, O. P., Inapagolla, R., Kannan, S., and Kannan, R. M. (2008) The effect of surface functionality on cellular trafficking of dendrimers. *Biomaterials 29*, 3469-3476.

(33) Albertazzi, L., Serresi, M., Albanese, A., and Beltram, F. (2010) Dendrimer Internalization and Intracellular Trafficking in Living Cells. *Mol. Pharmaceutics 7*, 680-688.

(34) Hong, S., Bielinska, A. U., Mecke, A., Keszler, B., Beals, J. L., Shi, X., Balogh, L., Orr, B. G., Baker Jr., J. R., and Banaszak Holl, M. M. (2004) Interaction of Poly(amidoamine) Dendrimers with Supported Lipid Bilayers and Cells: Hole Formation and the Relation to Transport. *Bioconjugate Chem. 15*, 774-782.

(35) Albertazzi, L., Storti, B., Marchetti, L., and Beltram, F. (2010) Delivery and Subcellular Targeting of Dendrimer-Based Fluorescent pH Sensors in Living Cells. *J. Am. Chem. Soc. 132*, 18158-18167.

(36) Kiessling, L. L., Young, T., Gruber, T. D., and Mortell, K. H. In *Glycoscience*; Fraser-Reid, Tatsuta and Thiem, Eds.; Springer: 2008, p 2483-2523.

(37) Dam, T. K., and Brewer, C. F. (2008) Effects of Clustered Epitopes in Multivalent Ligand-Receptor Interactions. *Biochemistry 47*, 8470-8476.

(38) Lundquist, J. J., and Toone, E. J. (2002) The Cluster Glycoside Effect. *Chem. Rev. 102*, 555-578.

(39) Imberty, A., Chabre, Y. M., and Roy, R. (2008) Glycomimetics and Glycodendrimers as High Affinity Microbial Anti-adhesins. *Chem. Eur. J. 14*, 7490-7499.

(40) Vrasidas, I., de Mol, N. J., Liskamp, R. M. J., and Pieters, R. J. (2001) Synthesis of Lactose Dendrimers and Multivalency Effects in Binding to the Cholera Toxin B Subunit. *Eur. J. Org. Chem. 2001*, 4685-4692.

(41) Arima, H., Yamashita, S., Mori, Y., Hayashi, Y., Motoyama, K., Hattori, K., Takeuchi, T., Jono, H., Ando, Y., Hirayama, F., and Uekama, K. (2010) In Vitro and In Vivo gene delivery mediated by Lactosylated Dendrimer/α-Cyclodextrin Conjugates (G2) into Hepatocytes. *J. Controlled Release 146*, 106-117.

(42) Hynes, R. O. (2002) Integrins: Bidirectional, Allosteric Signaling Machines. *Cell 110*, 673-687.

(43) Desgrosellier, J. S., and Cheresh, D. A. (2010) Integrins in cancer: biological implications and therapeutic opportunities. *Nat. Rev. Cancer 10*, 9-22.

(44) Welsh, D. J., and Smith, D. K. (2011) Comparing dendritic and self-assembly strategies to multivalency-RGD peptide-integrin interactions. *Org. Biomol. Chem. 9*, 4795-4801, and references therein.

(45) Burke, P. A., DeNardo, S. J., Miers, L. A., Lamborn, K. R., Matzku, S., and DeNardo, G. L. (2002) Cilengitide Targeting of αvβ3 Integrin Receptor Synergizes with Radioimmunotherapy to Increase Efficacy and Apoptosis in Breast Cancer Xenografts. *Cancer Res. 62*, 4263-4272.

(46) Mas-Moruno, C., Rechenmacher, F., and Kessler, H. (2010) Cilengitide: The First Anti-Angiogenic Small Molecule Drug Candidate. Design, Synthesis and Clinical Evaluation. *Anti-Cancer Agents Med. Chem. 10*, 753-768.

(47) Reardon, D. A., Neyns, B., Weller, M., Tonn, J. C., Nabors, L. B., and Stupp, R. (2011) Cilengitide: an RGD pentapeptide αvβ3 and αvβ5 integrin inhibitor in development for glioblastoma and other malignancies. *Future Oncol. 7*, 339-354.

(48) Rajendran, L., Knölker, H.-J., and Simons, K. (2010) Subcellular targeting strategies for drug design and delivery. *Nat. Rev. Drug Discov. 9*, 29-42.

(49) Ulbrich, K., and Subr, V. (2004) Polymeric anticancer drugs with pH-controlled activation. *Adv. Drug Delivery Rev. 56*, 1023-1050.